RESEARCH ARTICLE

small methods
www.small-methods.com

Design of Self-Standing Chiral Covalent-Organic Framework Nanochannel Membrane for Enantioselective Sensing

*Chen-Yan Zheng, Hai-Long Qian, Cheng Yang, and Xiu-Ping Yan**

Nanochannel membranes are promising materials for enantioselective sensing. However, it is difficult to make a compromise between the selectivity and permeability in traditional nanochannel membranes. Therefore, new types of nanochannel membranes with high enantioselectivity and excellent permeability should be explored for chiral analysis. Here, asymmetric catalysis strategy is reported for interfacial polymerization synthesis of chiral covalent-organic framework (cCOF) nanochannel membrane for enantioselective sensing. Chiral phenylethylamine (*S*/*R*-PEA) and 2,4,6-triformylphloroglucinol (TP) are used to prepare chiral TP monomer. 4,4′,4″-triaminotriphenylamine (TAPA) is then condensed with chiral TP to obtain cCOF nanochannel membrane via a C═N Schiff-base reaction. The molar ratio of TP to *S*/*R*-PEA is adjusted so that *S*/*R*-PEA is bound to the aldehyde only or both the aldehyde and hydroxyl groups on TP to obtain chiral-induced COF (cCOF-1) or both chiral-induced and modified COF (cCOF-2) nanochannel membrane, respectively. The prepared cCOF-2 nanochannel membrane showed two times more selectivity for limonene enantiomers than cCOF-1 nanochannel membrane. Furthermore, cCOF-2 nanochannel platform exhibited excellent sensing performance for other chiral molecules such as limonene, propanediol, methylbutyric acid, ibuprofen, and naproxen (limits of detection of 19–42 ng L^{-1}, enantiomer excess of 63.6–86.3%). This work provides a promising way to develop cCOF-based nanochannel enantioselective sensor.

1. Introduction

Chirality is a fundamental property of biomolecules in nature.[1] A chiral molecule cannot be superimposed on its mirror image and two non-identical mirror images are a pair of enantiomers.[2] Chiral enantiomers possess almost identical physicochemical properties in most inanimate environments but significant differences in medical science, food safety, and biological systems.[3] For instance, *S*-ketamine has a higher anesthetic effect than *R*-ketamine,[4] while only the *RR* enantiomer of chloramphenicol possesses antimicrobial properties.[5] In addition, chiral molecules are promising for various potential applications, such as enantiomeric separation, asymmetric catalysis, and chiroptical effects.[6] It is thus essential to detect the absolute configuration of chiral molecules in their precise applications.

A diversity of materials and techniques have been developed for chiral detection, including high-performance liquid chromatography (HPLC),[7] capillary electrophoresis,[8] circular dichroism (CD) spectroscopy,[9] and electrochemistry.[10] Among them, HPLC is a well-recognized technique for enantiomer recognition and separation because of its preparative-scale capabilities. HPLC generally exhibits a high efficiency with good selectivity, but traditional HPLC suffers from impossible high throughput analysis in the detection of chiral molecules at low concentrations owing to its relatively low sensitivity. Therefore, it is still necessary to develop a highly enantioselective method for sensitive detection of chiral molecules.

Nanochannel techniques stand out among various developed methods for analytes owing to the advantages of high sensitivity, high throughput, low cost, and simple use.[11] Artificial solid-state nanochannels have attracted extensive attention due to their adjustable geometry and dimension, easy functionalization, and excellent mechanical stability.[12] Recent studies show that introducing various functional chiral ligands onto nanochannel surfaces gave good selective recognition and transport performance for chiral analytes.[13] Feng et al. incorporated a chiral pillar[6]arene functionalized gold nanoparticles (AuNPs) into the polycarbonate membrane to design a nanochannel for highly selective enantioseparation of amino alcohols.[13a] Zhang et al. prepared an artificial nanochannel with antiporter behavior for

C.-Y. Zheng, H.-L. Qian, X.-P. Yan
State Key Laboratory of Food Science and Resources
Jiangnan University
Wuxi 214122, China
E-mail: xpyan@jiangnan.edu.cn
C.-Y. Zheng, H.-L. Qian, X.-P. Yan
International Joint Laboratory on Food Safety
Jiangnan University
Wuxi 214122, China
C.-Y. Zheng, H.-L. Qian, C. Yang, X.-P. Yan
Institute of Analytical Food Safety
School of Food Science and Technology
Jiangnan University
Wuxi 214122, China
X.-P. Yan
Key Laboratory of Synthetic and Biological Colloids
Ministry of Education
Jiangnan University
Wuxi 214122, China

The ORCID identification number(s) for the author(s) of this article can be found under https://doi.org/10.1002/smtd.202401120

DOI: 10.1002/smtd.202401120

chiral sensing and separation.[13b] Yang et al. reported a gating nanochannel for sensitive identification of chiral drugs by introducing L-amino acids into biomimetic nanochannels.[13c] However, the relatively small surface area and low permeability of existing functionalized biomimetic polymer nanochannel membranes may significantly reduce the nanochannel performance, leading to unsatisfactory nanochannel application.[14] Therefore, exploring new types of nanochannel membranes with high enantioselectivity and excellent permeability is conducive to develop advanced nanochannel systems for chiral analysis.

Covalent-organic frameworks (COFs) have drawn extensive attention in nanochannel applications such as catalysis,[15] separation,[16] sensing,[17] and ion transport[18] for their ordered structure, large specific surface area and controllable pore size. To date, few researchers have incorporated COF into artificial solid-state nanochannels to develop chiral nanochannel platforms. Yuan et al. prepared a mixed matrix membranes containing β-cyclodextrin-modified COF for enantioselective sensing of amino acids.[19] However, the content of COF in the mixed matrix membrane hardly exceeds 50%, failing to fully exploit the advantages of the ordered pores of COF.[20] Zhang et al. reported L-tyrosine-COF packed polyethylene terephthalate nanochannel for high-throughput and selective enantioseparation of naproxen.[21] Nevertheless, the limited and inhomogeneous recognition sites led to low molecular selectivity.[22] The COF membranes synthesized via interfacial polymerization not only possess the advantages of flexibility and defect-free but also exhibit the benefits of adjustable thickness and ease of transfer.[23] Our group designed a pure COF nanochannel sensor with a chiral AuNPs selector.[24] However, the reaction rate and selectivity of chemical reactions outside the nanochannels are lower than those inside the nanochannels.[25] Therefore, the incorporation of chiral functional groups into COF membranes is a good strategy for constructing chiral nanochannel platforms.

Chiral COF (cCOF) with uniform chiral active sites has exhibited diverse potential applications in asymmetric catalysis and enantioselective separation.[26] cCOFs can be used as a host for chiral molecule recognition through precise adjustment of their pore size and surface groups. Moreover, the intrinsic space confinement effect within cCOF pores can enhance the interaction between host and guest. As a bridge between nanosystem and macroscopic object, cCOF membrane with 1D nanochannel not only easily exposes chiral recognition sites, but also effectively shortens mass transfer to improve the enantioselectivity of cCOF.[14,27] Thus, cCOF membrane is a good candidate for constructing a chiral nanochannel sensor platform. To the best of our knowledge, cCOF membrane-based chiral nanochannel platforms have not been explored so far.

Herein, we propose an asymmetric catalysis strategy for interfacial polymerization to fabricate cCOF nanochannel membrane sensor for the highly enantioselective sensing. Chiral phenylethylamine (*S*/*R*-PEA) and 2,4,6-triformylphloroglucinol (TP) were used to prepare chiral TP monomer for subsequent condense with 4,4′,4″-triaminotriphenylamine (TAPA) to obtain cCOF nanochannel membrane via C═N Schiff-base reaction. Notably, the molar ratio of TP to *S*/*R*-PEA was adjusted the binding of *S*/*R*-PEA to the aldehyde only or both the aldehyde and hydroxyl groups on TP to obtain chiral-induced nanochannel membrane (cCOF-1) or both chiral-induced and modified nanochannel membrane (cCOF-2), respectively. The prepared cCOF-2 nanochannel membrane showed much more enantioselective than cCOF-1 nanochannel membrane. This study paves an avenue to the preparation of cCOF membrane nanochannel for highly enantioselective sensing.

2. Results and Discussion

2.1. Design and Synthesis of the cCOF Nanochannel Membranes

Figure 1 illustrates the design, preparation, and ion transport of the cCOF nanochannel membrane using *S*-PEA. The stable β-ketoenamine-linked cCOF nanochannel membranes were synthesized via asymmetric catalysis of interfacial polymerization. A TP to *S*-PEA molar ratio less than 1:3 preferred the reaction of the amino groups on *S*-PEA and the aldehyde groups on TP to form chiral TP-1 (Figures S1 and S2a, Supporting Information), then the *S*-PEA in chiral TP-1 was dynamically exchanged with TAPA to leave imprinted chiral memory sites, and ultimately to form chiral-induced nanochannel membrane (cCOF-1-*S*-PEA). When the molar ratio of TP to *S*-PEA was greater than 1:3, the amino groups on *S*-PEA reacted with both the aldehyde and hydroxyl groups to modify TP to form chiral TP-2 (Figures S3 and S2b, Supporting Information). In this case, the *S*-PEA in chiral TP-2 not only was dynamically exchanged with TAPA to leave imprinted chiral memory sites, but also provided chiral groups to TP, and finally formed both chiral-induced and modified nanochannel membrane (cCOF-2-*S*-PEA). Moreover, the achiral COF was selected as a contrast nanochannel membrane.

The organocatalytic asymmetric Schiff-base condensation can be conducted under room temperature and atmospheric pressure, and the achiral monomers are directly transformed into cCOF in the presence of a chiral organic catalyst.[6b,28] Thus, an organic-aqueous reaction system was exploited with TAPA aqueous solution while the TP and *S*-PEA in dichloromethane (DCM) to manipulate the polymerization process of the COF for chiral membranes preparation (Figure 1b). The prepared self-standing cCOF membranes with aligned 1D nanochannel are excellent candidates for efficient ion transport nanochannel membranes (Figure 1c).

2.2. Characterization of the cCOF Nanochannel Membranes

The synthesized COF nanochannel membranes (achiral COF, cCOF-1-*S*-PEA, and cCOF-2-*S*-PEA) were characterized by powder X-ray diffraction (PXRD), Fourier transform infrared (FT-IR) and solid-state circular dichroism (CD) spectroscopy as well as contact angle measurement. The experimental diffraction peaks at 2θ = 6.84°, 6.90°, and 6.74° for all the synthesized COF nanochannel membranes agreed well with the peaks simulated from AA stack model (Figure S4a, Supporting Information), suggesting the successful synthesis of the 1D COF nanochannel membranes. It is noteworthy that the crystallinity of the β-ketoenamine-linked COF membrane synthesized via interfacial polymerization is significantly inferior to that synthesized by solvothermal method.[29] The appearance of the FT-IR peak at

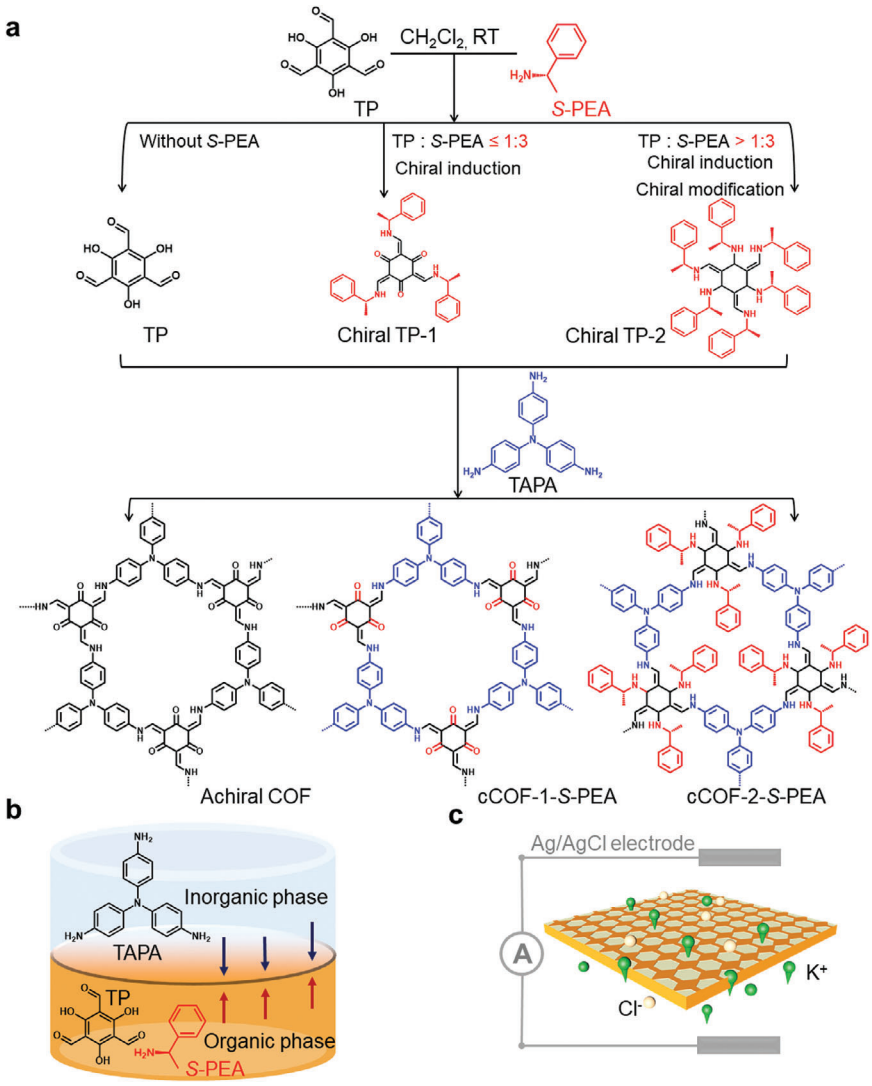

Figure 1. a) Schematic for the synthesis of cCOFs-*S*-PEA. b) Schematic of the organic-aqueous reaction system for preparing cCOFs-*S*-PEA nanochannel membranes. c) Illustration for ion transport base on the cCOFs nanochannel membranes.

1596–1609 cm^{-1} (C═C) and 1265–1271 cm^{-1} (C—N) confirmed the formation of the *β*-ketoenamine. Meanwhile, the absence of N—H and —C═O stretching bonds at 3337–3404 and 1643 cm^{-1}, respectively, suggests no residual of the starting precursors in the formed COF nanochannel membranes.

The FT-IR spectra, contact angles, and the solid-state ^{13}C cross-polarization/magic angle spinning nuclear magnetic resonance (CP-MAS NMR) spectra of the as-prepared cCOF-1-*S*-PEA nanochannel membrane were very similar to those for the achiral COF nanochannel membrane (Figures S4b,c and S5a, Supporting Information), because of the dynamic amine exchange among *S*-PEA and TAPA.[28] Notably, the appearance of the new peak at 1388 cm^{-1} (—CH_3) in the FT-IR spectra (Figure S4b, Supporting Information) and the carbon signals at 20–57 ppm in the solid-state ^{13}C CP-MAS NMR spectra (Figure S5b, Supporting Information) of cCOF-2-*S*-PEA nanochannel membrane verified the successful modification of *S*-PEA. In addition, the contact angle of the cCOF-2-*S*-PEA nanochannel membrane (77.2 ± 0.1°) was greater than that of the cCOF-1-*S*-PEA nanochannel membrane (69.6 ± 0.2°) (Figure S4c, Supporting Information), while the pore size (0.5 nm) was smaller than that (1.1 nm) of the cCOF-1-*S*-PEA nanochannel membrane (Figure S6, Supporting Information), likely because of the modification of the benzene ring and methyl group of *S*-PEA in the cCOF-2-*S*-PEA nanochannel membrane.

The photos, atomic force microscopy (AFM), and top-view scanning electron microscopy (SEM) images of the COF nanochannel membranes are shown in Figure S7 (Supporting Information). These COF nanochannel membranes could naturally stretch in water for nanofluidic applications (Figure S7a, Supporting Information). The surface roughness of the membrane was less than 2.3 nm, indicating the smooth surface of the COF membranes (Figure S7b, Supporting Information). In addition, these COF nanochannel membranes were continuous without any cracks in the top-view of the membranes (Figure S7c, Supporting Information). Moreover, the as-prepared

cCOF-1/2-*S*/*R*-PEA nanochannel membranes had optical activity and displayed Cotton effects in the wavelength range of 240–800 nm in the solid-state CD spectra (Figure S8, Supporting Information). The cCOF-1-*S*/*R*-PEA nanochannel membrane synthesized by chiral induction had an obvious CD signal at 250 nm, while the cCOF-2-*S*/*R*-PEA nanochannel membrane synthesized by both chiral induction and modification had a weak and strong CD signal at 250 and 607 nm, respectively. The above results indicate the successful synthesis of achiral COF, cCOF-1-*S*-PEA (chiral induction), and cCOF-2-*S*-PEA (chiral induction and modification) nanochannel membranes.

2.3. Ionic Transport Performance of cCOF-*S*-PEA Nanochannel Membrane

The ion selectivity and the surface-charge-governed ion transport of the nanochannel membrane are important bases for highly enantioselective sensing.[30] As such, the ion transport properties of the cCOF-1-*S*-PEA and cCOF-2-*S*-PEA nanochannel membranes were obtained on a homemade Teflon electrolytic cell with a pair of Ag/AgCl electrodes.[31] The cCOF-1-*S*-PEA and cCOF-2-*S*-PEA membrane exhibited an effective ion-transporting area of 2.5 mm^2. The cCOF-1-*S*-PEA and cCOF-2-*S*-PEA nanochannel membranes were first soaked in the corresponding KCl solution for 12 h, and then the *I*–*V* test was repeated three times to obtain the steady-state current. The currents of the cCOF-1-*S*-PEA and cCOF-2-*S*-PEA nanochannel membranes were recorded in the range of −0.2 to 0.2 V in KCl solution from 10^{-9} to 1 M (Figure S9a,b, Supporting Information). The ionic conductance at various KCl solutions revealed that the ion transport was governed by surface charge in low-concentration ($<10^{-5}$ M) of KCl solutions (Figure S9c,d, Supporting Information).[30] Meanwhile, the nanochannel sizes of the as-prepared cCOF-1-*S*-PEA (1.1 nm) and cCOF-2-*S*-PEA (0.5 nm) nanochannel membranes were notably inferior to the Debye length in 10^{-6} M KCl solution (305 nm), indicating that the as-fabricated nanochannels were fully negatively charged, and K^+ was the main charge carrier (Figure S9e, Supporting Information).[32] Moreover, no obvious change of the *I*–*V* curves of the as-prepared cCOF-1-*S*-PEA and cCOF-2-*S*-PEA nanochannel membranes in 0.1 μM KCl solution for 5 days indicates the good stability of the proposed nanochannel membranes (Figure S9f,g, Supporting Information). In addition, the nanochannel membranes of cCOF-1-*S*-PEA and cCOF-2-*S*-PEA had good stability in strong acid, strong alkali, and high-temperature environments (Figure S9h–j, Supporting Information). There was no significant change in the current value at 0.2 V over 30 cycles, indicating the good reusability of the prepared cCOF-1-*S*-PEA and cCOF-2-*S*-PEA membranes (Figure S10, Supporting Information). Therefore, 0.1 μM KCl solution was chosen as the supporting electrolyte for further chiral sensing.

2.4. Chiral Sensing

The operation principle of this chiral sensing system is shown in Figure S11 (Supporting Information). The cCOF-1-*S*-PEA and cCOF-2-*S*-PEA nanochannel membranes in the KCl solution work as ion transport channels for K^+ and chiral receptors. Selective binding of one enantiomer to the surface and inner wall of the as-prepared nanochannel membrane disrupts the ion transport of the channel surface, leading to a change in the transmembrane ion current. Thus, the chiral sensing of the enantiomers can be achieved by measuring the transmembrane ion current of the cCOF-1-*S*-PEA and cCOF-2-*S*-PEA nanochannel membranes in KCl solution (0.1 μM, pH 7.14).

Limonene enantiomers were chosen to demonstrate the performance of the prepared COF nanochannel membranes for chiral sensing. Since *R*-limonene is a major component in various citrus fruits, spices, and herbs, cCOF-1/2-*S*-PEA membrane was chosen as a nanochannel sensor to demonstrate their chiral sensing performance for limonene enantiomers. Obviously, the cCOF-1-*S*-PEA and cCOF-2-*S*-PEA nanochannel membranes enabled selective sensing of limonene enantiomers (**Figure 2**a–d), but the achiral COF nanochannel membrane did not (Figure 2c,d). The selectivity for the nanochannel was calculated from the ratio of the current change rate for the limonene enantiomers, i.e., $\Delta I_R/\Delta I_S$, where $\Delta I = (I_0 - I)/I_0$. The cCOF-2-*S*-PEA nanochannel membrane gave a selectivity of 11.6 for limonene enantiomers (Figure 2d), two times more than that (3.9) of the cCOF-1-*S*-PEA nanochannel membrane (Figure 2d). Molecular docking analysis demonstrated the existence of van der Waals forces between cCOF-1/2-*S*-PEA and limonene at the molecular level. In addition, cCOF-2-*S*-PEA had a greater affinity to (*R*)-limonene (−6.03 kcal mol^{-1}) than cCOF-1-*S*-PEA (−4.52 kcal mol^{-1}) (**Figure 3**). The large and negative binding energy of (*R*)-limonene indicated a favorable binding of (*R*)-limonene to cCOF-2-*S*-PEA. Based on the above results, the cCOF-2-*S*-PEA nanochannel membrane was selected for further sensing experiments.

The performance of the cCOF-2-*S*-PEA for sensing limonene enantiomers was further explored. Figure S12 (Supporting Information) shows the relationship between the transmembrane ion current intensity and the concentration of limonene enantiomers. As the concentration of limonene enantiomers increased, the transmembrane ion currents at 0.2 V for (*R*)-limonene obviously dropped (Figure S12a, Supporting Information), whereas it remained almost constant for (*S*)-limonene (Figure S12b, Supporting Information). Meanwhile, a good linear response of ΔI to (*R*)-limonene concentration was observed within the concentration range of 100 ng L^{-1}–0.5 mg L^{-1} ($\Delta I = 5.35 \lg(C_{(R)\text{-limonene}}) + 21.54$, $R^2 = 0.9740$) (Figure S13, Supporting Information). In addition, a low limit of detection (LOD) of 19 ng L^{-1} (S/N = 3) was achieved. The intra-assay and inter-assay precisions (RSD, n = 6) for the sensing of (*R*)-limonene were in the range of 3.9–4.6% and 3.7–4.4%, respectively (Table S1, Supporting Information), indicating the good repeatability and reproducibility of the as-prepared chiral sensing platform. The developed cCOF-2-*S*-PEA nanochannel sensor was also compared with other reported sensors (Table S2, Supporting Information), showing a wider linear range and a lower LOD than other reported sensors.[24,34] It is noteworthy that the cCOF-2-*R*-PEA nanochannel membrane exhibited opposite enantioselectivity, showing good sensing performance for (*S*)-limonene (Table S3, Supporting Information). Besides, no significant change in the sensitivity of cCOF-2-*S*-PEA nanochannel sensor for (*R*)-limonene was observed in the presence of (*S*)- limonene, and vice

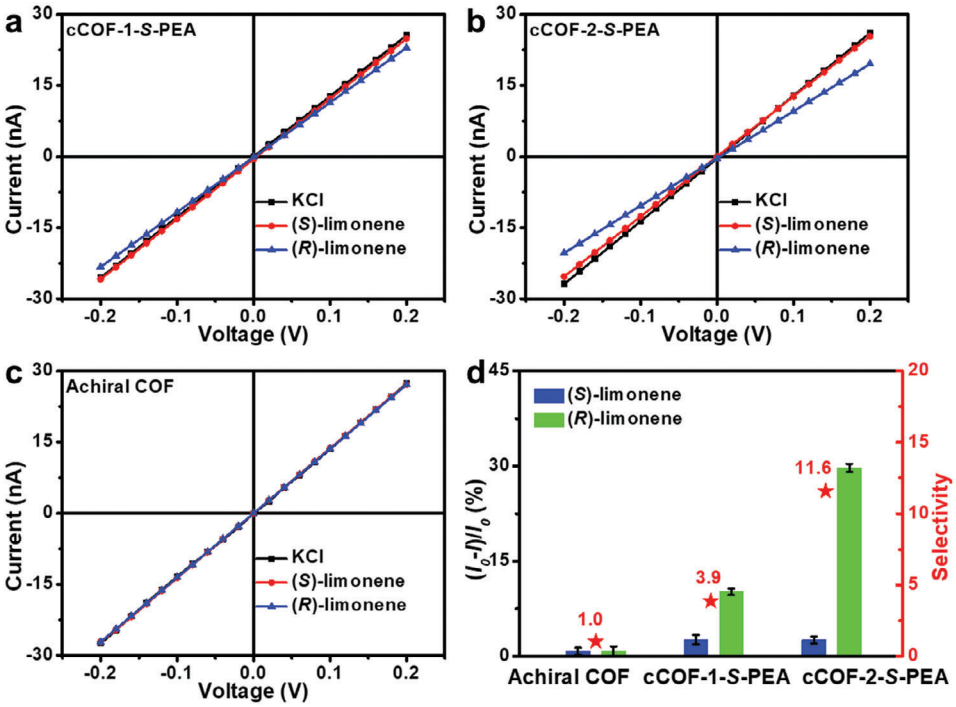

Figure 2. *I*–*V* plots in 0.1 μM KCl solution at pH 7.14 with and without limonene enantiomers (1 mg L^{-1}): a) cCOF-1-*S*-PEA nanochannel membrane; b) cCOF-2-*S*-PEA nanochannel membrane; c) Achiral COF nanochannel membrane. d) Current change rate and selectivity for a–c. *I* and I_0 refer to the current at 0.2 V with and without limonene enantiomer, respectively. Data are shown as mean ± SD ($n = 3$).

versa (Figure S13, Supporting Information). Thus, both cCOF-2-*S*-PEA and cCOF-2-*R*-SEA nanochannel sensors enable the quantitation of (*R*/*S*)-limonene in a sample.

2.5. Enantioselective Mechanism

The enantioselective mechanism of cCOF-2-*S*-PEA nanochannel membrane to limonene was explored by zeta potential and current–time (*I*–*t*) test. The zeta potential of the achiral COF and cCOF-2-*S*-PEA nanochannel membrane was −6.07 and −5.43 mV, respectively (**Figure** 4a). Immersing the achiral COF nanochannel membrane into 1 mg L^{-1} (*S*)- and (*R*)-limonene solutions overnight made no significant change in zeta potential. However, the cCOF-2-*S*-PEA nanochannel membrane became less negative zeta potential (−5.17 and −3.42 mV for (*S*)-limonene and (*R*)-limonene, respectively) after its overnight immersion in 1 mg L^{-1} (*S*)- and (*R*)-limonene solutions. The van der Waals forces between cCOF-2-*S*-PEA and (*R*)-limonene induced the aggregation of cCOF-2-*S*-PEA. This result indicates that the *S*-PEA of the cCOF-2-*S*-PEA nanochannel membrane possessed stronger binding with (*R*)-limonene than (*S*)-limonene, and the *S*-PEA with (*R*)-limonene could reduce negative charge density of the membrane surface.

The *I*–*t* test was performed to further demonstrate the dynamic change in the current of the cCOF-2-*S*-PEA nanochannel membrane with limonene enantiomers. Addition of 1 mg L^{-1} (*S*)- or (*R*)-limonene solution to 0.1 μM KCl solution led to a similar current change of achiral COF nanochannel membrane (Figure 4b), but a significant difference in the current change of cCOF-2-*S*-PEA nanochannel membrane (Figure 4c). Again, this result indicates that the binding of (*R*)-limonene with *S*-PEA reduced more negative surface charge of the cCOF-2-*S*-PEA nanochannel membrane.

The concentration distribution of (*S*)- and (*R*)-limonene in the cCOF-2-*S*-PEA nanochannel membrane was then studied. For this purpose, COMSOL Multiphysics 6.0 was used to build a steady-state finite simulation model. The concentration distribution of (*S*)- and (*R*)-limonene in the cCOF-2-*S*-PEA nanochannel was theoretically computed via finite-element simulation. (*R*)-limonene showed a larger concentration gradient in the cCOF-2-*S*-PEA nanochannel than (*S*)-limonene (Figure 4d), indicating that the cCOF-2-*S*-PEA nanochannel had a better recognition ability of (*R*)-limonene.

2.6. Universality of the cCOF-2 Nanochannel Platform for Enantioselective Sensing

To demonstrate the universality of the as-prepared cCOF-2 nanochannel membrane, four representative chiral molecules were selected for enantioselective sensing. As for the as-prepared cCOF-2-*S*-PEA nanochannel membrane, *R*-enantiomers of each pair of enantiomers exhibited more significant change in the transmembrane ion current than *S*-enantiomers (Figures S14–S17, Supporting Information), and the current change rate of the *R*-enantiomers was much higher than that of the *S*-enantiomers (**Table** 1). Moreover, the as-prepared cCOF-2-*S*-PEA nanochannel sensor exhibited highly enantioselective sensing capability between all enantiomers with the selectivity of

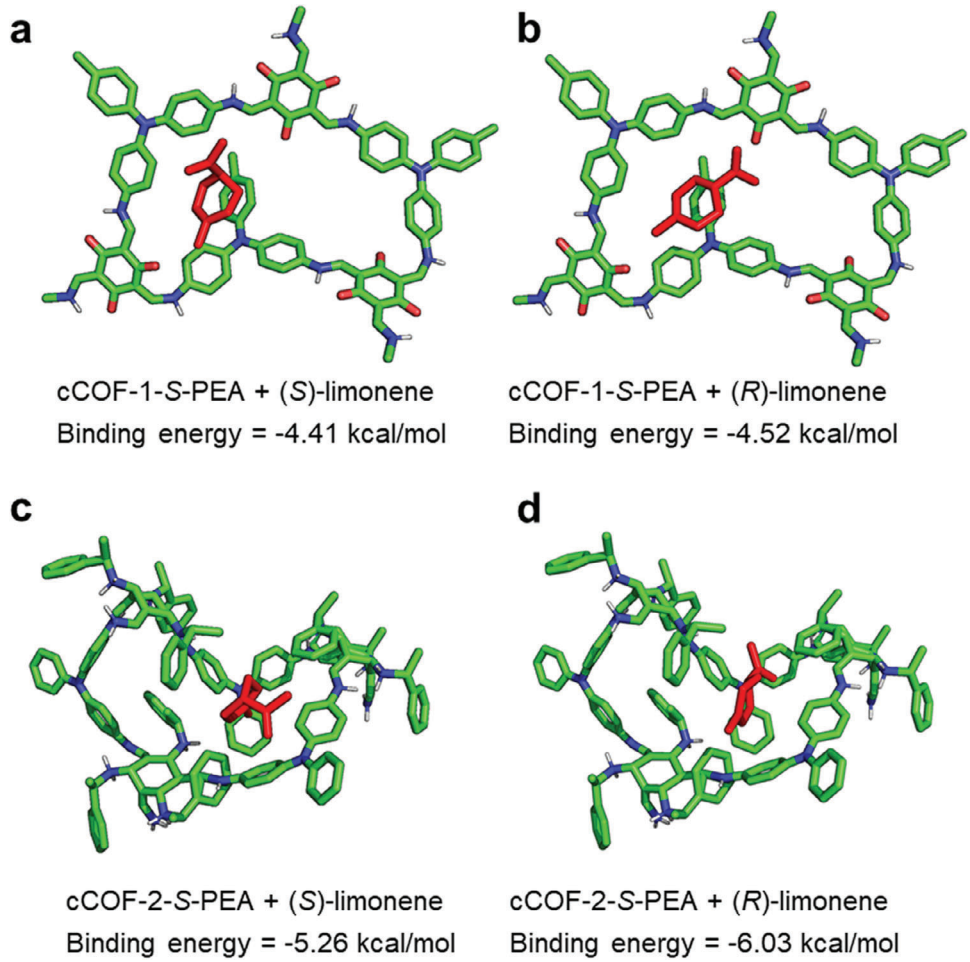

Figure 3. Interaction modes and binding energies between cCOF-1/2-*S*-PEA and limonene enantiomers.

4.3 (ibuprofen), 5.2 (propanediol), 5.4 (methylbutyric acid), 8.7 (naproxen) and 11.6 (limonene) (Table 1). The above results show that the as-prepared cCOF-2-*S*-PEA nanochannel platform can be applied to the sensing of other chiral molecules. Additionally, a good linear relationship between ΔI value and the logarithm of the concentrations of enantiomers was observed within the concentration range of 0.1 μg L^{-1}–0.5 mg L^{-1} (Table S3, Supporting Information LOD: 19–42 ng L^{-1}; ee: 63.6–86.3%).

2.7. Real Sample Analysis

Sweet orange oil and lemon oil are essential fragrant raw materials in the composition of citrus fragrances, while limonene is a crucial component affecting the sensory quality of lemon oil and sweet orange oil. Therefore, the proposed cCOF-2-*S*/*R*-PEA nanochannel sensors were applied for the determination of (*R*/*S*)-limonene enantiomers in citrus fragrances for evaluating its practicability. The results obtained by our cCOF-2 nanochannel sensors are summarized and compared with those obtained by a chiral gas chromatography-mass spectrometry (GC-MS) method in Table S4 (Supporting Information). The results show that no (*S*)-limonene in the oil samples studied was detected by the developed cCOF-2 nanochannel sensor. However, the concentrations of (*R*)-limonene in the studied oil samples were found to be in the range of 41–536 mg g^{-1} with good precision (3.5–4.3% RSD (n = 3)), in good agreement with those obtained by GC-MS method. The above results show the feasibility of the proposed method for the determination of (*R*/*S*)-limonene enantiomers in real samples.

3. Conclusion

In summary, we have reported asymmetric catalysis of interfacial polymerization fabrication of cCOF nanochannel membrane for enantioselective sensing. Selective binding of one enantiomer to the cCOF nanochannel membrane with uniform chiral active sites disrupts the channel surface ion transport and achieves enantioselective sensing. The as-prepared cCOF nanochannel membrane not only exposes uniform chiral recognition sites, but also overcomes the inherent difficulty in balancing permeability and selectivity of traditional polymer nanochannel membranes for enantioselective sensing. This work demonstrates the merits of cCOF membranes in the preparation of enantioselective nanochannel membrane materials, and opens a new way for the

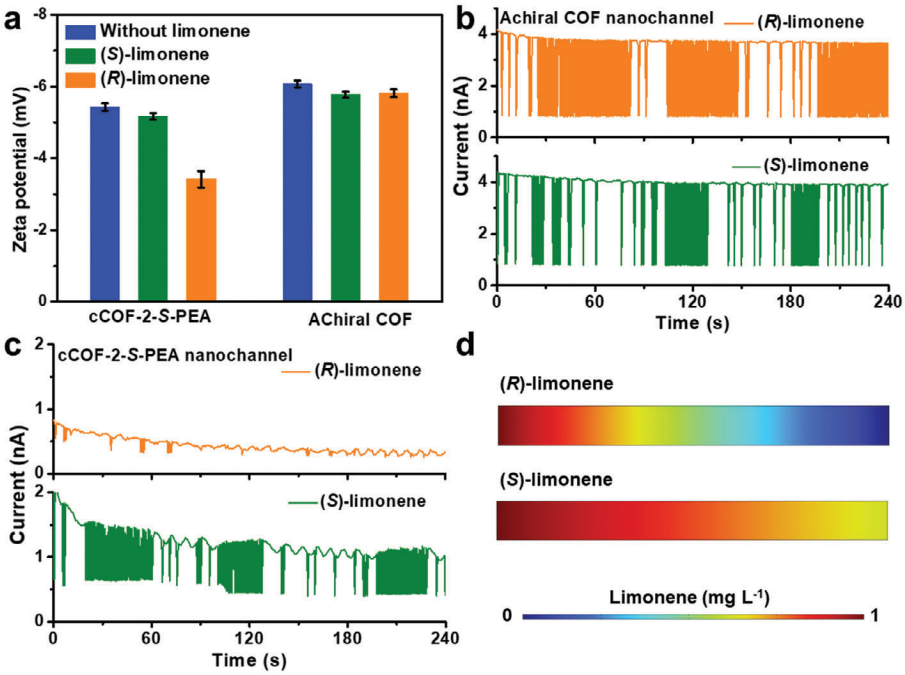

Figure 4. a) Change in zeta potential after the nanochannel bound to limonene enantiomers. *I*–*t* curves in KCl solution (0.1 μM, pH 7.14) with 1 mg L^{-1} (*S*)- and (*R*)-limonene. Data are shown as mean ± SD ($n = 3$). b) Achiral COF and c) cCOF-2-*S*-PEA nanochannel membrane. d) Simulated concentration distribution of limonene enantiomers in the cCOF-2-*S*-PEA nanochannel membrane.

design of the chiral nanochannel sensors for highly enantioselective sensing.

4. Experimental Section

Materials and Chemicals: Ultrapure water was from Wahaha Group Co. (Hangzhou, China). TP and TAPA came from Yanshen Technology Co. (Changchun, China). KCl, acetone, DCM, and acetic acid (HAc) were obtained from Sinopharm Chemical Reagent Co. (Shanghai, China). *S*/*R*-PEA, *S*/*R*-limonene, *S*/*R*-propanediol, *S*/*R*-methylbutyric acid, *S*/*R*-butanol, *S*/*R*-ibuprofen, and *S*/*R*-naproxen were provided by Aladdin Chemistry Co. (Shanghai, China).

Preparation of COF Nanochannel Membranes: All three COF nanochannel membranes, the achiral COF, cCOF-1, and cCOF-2, were synthesized in a glass beaker by controlling the addition of *S*/*R*-PEA. The COF nanochannel membranes were prepared according to previous methods with little modification.[6b,28,33] First, a mixture of TP (0.06 mmol) and *S*-PEA (0, 0.06, and 0.20 mmol for the achiral COF, cCOF-1-*S*-PEA and cCOF-2-*S*-PEA, respectively) in DCM (10 mL) was sonicated for 10 min to give a clear and yellow solution. Then, ultrapure water (5 mL) was added dropwise to the aldehyde solution as a spacer layer. Subsequently, TAPA (0.06 mmol) was dissolved in ultrapure water (5 mL) and added dropwise to the spacer solution. Afterward, the catalyst HAc (3.0 M, 120 μL) was slowly added to the mixture. The glass beaker was covered with a cling film for 72 h interfacial polymerization at room temperature and atmospheric pressure. The COF nanochannel membranes formed at the interface were carefully taken out from the beaker with tweezers. Then, the COF nanochannel membranes were soaked in acetone and ultrapure water, in turn, to purify the membranes and eventually stored in ultrapure water for further experiments. Similarly, the replacement of *S*-PEA by *R*-PEA resulted in the synthesis of cCOF-1-*R*-PEA and cCOF-2-*R*-PEA nanochannel membranes.

Table 1. Selectivity and current change rate of the cCOF-2-*S*-PEA nanochannel platform for different chiral molecules.

Chiral molecules	Current change rate	Selectivity
(*R*/S)-limonene	29.7/2.6	11.6
(*R*/S)-1,2-propanediol	12.6/2.4	5.2
(*R*/*S*)-2-methylbutyric acid	12.7/2.3	5.4
(*R*/*S*)-ibuprofen	11.2/2.6	4.3
(*R*/*S*)-naproxen	20.7/2.4	8.7

Instrumentation: PXRD patterns were recorded on a D2 PHASER X-ray diffractometer (Bruker, Germany) with Cu K*α* radiation in the range from 2° to 40° at a scanning speed of 8° min^{-1}. FT-IR spectra were collected on a Nicolet IS20 spectrometer (Nicolet, USA). Samples for FT-IR were prepared as KBr pellets. Contact angles were measured on an OCA15EC contact angle system (DataPhysics, Germany) at 25 °C and saturated humidity. Solid ^{13}C NMR experiments were carried out on a Bruker Avance III HD 400 MHz NMR (Bruker, Germany). N_2 adsorption/desorption experiments were performed on an Autosorb-iQ analyzer (Quantachrome, USA) at 77 K. AFM measurements were conducted on a Dimension FastScan analyzer (Bruker, Germany). SEM images were acquired on an SU8100 instrument (Hitachi, Japan) at 3.0–5.0 kV. The solid-state CD spectra were obtained on Chirascan V100 (Applied Photophysics, U.K.). The zeta potentials were determined on a Nano ZS system (Malvern, U.K.). An Agilent 7890B gas chromatograph coupled with an Agilent 7000D mass spectrometer (Agilent Technologies, Palo Alto, CA) was used for the analysis. A CYCLOSIL-B column (30 m×0.25 mm i.d.) was used for chiral separation. A homemade nanochannel analysis platform, as described in the previous work,[31] was employed for chiral sensing.

Molecular Docking Analysis: AutoDock 1.5.7 was employed to evaluate the interaction modes and binding affinities of the cCOFs and chiral molecules. The molecular structures of chiral molecules were obtained

from PubChem database, accessible at https://pubchem.ncbi.nlm.nih.gov/.

Finite-Element Simulation: COMSOL Multiphysics 6.0 was utilized for the steady-state finite element simulation to establish a quantitative model for the highly enantioselective transport. Three modules, i.e., laminar flow (spf), electrostatics (es), transport of diluted species (chds), were employed to simulate the enantioselective transport. The nanoscale dimensions of the COF nanochannel membrane were characterized as 50 nm in diameter (Φ) and 500 nm in length (L), with each cross-sectional axis including 100 COF channels. The diffusion rate of limonene enantiomers was derived based on their transport rate ((*S*)- limonene: 2.12×10^{-8} m^2 s^{-1}; (*S*)- limonene: 5.36×10^{-5} m^2 s^{-1}).

Pretreatment of Real Samples: Sweet orange oil and lemon oil were purchased from a local supermarket. The sample (20 mg) was dissolved in 2 mL of methanol, and shaken at 150 rpm for 5 min. Then, the mixture was filtered with a 0.22 µm filter membrane and diluted 1000 times with methanol for the determination of limonene enantiomers by the developed nanochannel sensor and GC-MS, respectively.

Supporting Information

Supporting Information is available from the Wiley Online Library or from the author.

Acknowledgements

This work was supported by the National Natural Science Foundation of China (no. 22176073), the Postgraduate Research & Practice Innovation Program of Jiangsu Province (no. KYCX23_2508), and the Program of "Collaborative Innovation Center of Food Safety and Quality Control in Jiangsu Province".

Conflict of Interest

The authors declare no conflict of interest.

Data Availability Statement

The data that support the findings of this study are available in the supplementary material of this article.

Keywords

chiral molecules, covalent-organic frameworks, enantioselective, nanochannels, sensing

Received: July 22, 2024
Revised: October 23, 2024
Published online:

[1] J. Gal, *Chirality* **2008**, *20*, 5.
[2] P. J. Ramberg, G. J. Somsen, *Ann. Sci.* **2010**, *58*, 51.
[3] a) Y. Wen, M. Q. He, Y. L. Yu, J. H. Wang, *Adv. Colloid Interface Sci.* **2021**, *289*, 102376; b) Y. P. Xue, C. H. Cao, Y. G. Zheng, *Chem. Soc. Rev.* **2018**, *47*, 1516; c) Y. Ruan, H. Lin, X. Zhang, R. Wu, K. Zhang, K. M. Y. Leung, J. C. W. Lam, P. K. S. Lam, *J. Hazard. Mater.* **2020**, *394*, 122589; d) S. E. Ebeler, in *Authentication of Food and Wine*, ACS Symposium Series, American Chemical Society, Washington, DC **2006**.
[4] A. Gergely, F. Zsila, P. Horváth, G. Szasz, *Chirality* **1999**, *11*, 741.
[5] B. J. A. Berendsen, T. Zuidema, J. de Jong, L. A. M. Stolker, M. W. F. Nielen, *Anal. Chim. Acta* **2011**, *700*, 78.
[6] a) B. Shen, Y. Kim, M. Lee, *Adv. Mater.* **2020**, *32*, 1905669; b) F. Li, J. L. Kan, B. J. Yao, Y. B. Dong, *Angew. Chem., Int. Ed.* **2022**, *61*, 202115044; c) H. Zhang, L. L. Lou, K. Yu, S. Liu, *Small* **2021**, *17*, 2005686.
[7] a) M. F. Alajmi, A. Hussain, M. Suhail, S. D. Mukhtar, D. R. Sahoo, L. Asnin, I. Ali, *Chirality* **2016**, *28*, 642; b) N. Y. Xu, P. Guo, J. K. Chen, J. H. Zhang, B. J. Wang, S. M. Xie, L. M. Yuan, *Talanta* **2021**, *235*, 122754.
[8] S. Bernardo-Bermejo, E. Sánchez-López, M. Castro-Puyana, M. L. Marina, *TrAC Trends Anal. Chem.* **2020**, *124*, 115807.
[9] Y. Zhao, A. N. Askarpour, L. Sun, J. Shi, X. Li, A. Alu, *Nat. Commun.* **2017**, *8*, 14180.
[10] a) J. Yang, Y. Yu, D. Wu, Y. Tao, L. Deng, Y. Kong, *Anal. Chem.* **2018**, *90*, 9551; b) Y. Yu, Y. Tao, B. Yang, D. Wu, Y. Qin, Y. Kong, *Anal. Chem.* **2017**, *89*, 12930; c) S. Ding, S. Cao, A. Zhu, G. Shi, *Anal. Chem.* **2016**, *88*, 12219.
[11] a) M. Cheng, F. Zhu, S. Zhang, X. Zhang, M. K. Dhinakaran, H. Li, *Nano Lett.* **2021**, *21*, 4086; b) Z. Zhu, D. Wang, Y. Tian, L. Jiang, *J. Am. Chem. Soc.* **2019**, *141*, 8658; c) X. Zhang, H. Liu, L. Jiang, *Adv. Mater.* **2019**, *31*, 1804508; d) J. A. Cooper, S. Borsley, P. J. Lusby, S. L. Cockroft, *Chem. Sci.* **2017**, *8*, 5005.
[12] a) R. Li, X. Fan, Z. Liu, J. Zhai, *Adv. Mater.* **2017**, *29*, 1702983; b) K. Xiao, L. Wen, L. Jiang, *Small* **2016**, *12*, 2810; c) X. Hou, *Adv. Mater.* **2016**, *28*, 7049; d) X. Kan, C. Wu, L. Wen, L. Jiang, *Small Methods* **2022**, *6*, e2101255.
[13] a) F. Feng, S. Zhang, L. Yang, G. Li, W. Xu, H. Qu, J. Zhang, M. K. Dhinakaran, C. Xu, J. Cheng, H. Li, *Anal. Chem.* **2022**, *94*, 6065; b) S. Zhang, M. Cheng, M. K. Dhinakaran, Y. Sun, H. Li, *ACS Nano* **2021**, *15*, 13148; c) L. Yang, Z. Sun, S. Zhang, Y. Sun, H. Li, *Small* **2023**, *19*, e2205274.
[14] M. Chen, X. Li, J. Li, C. Liu, A. Yu, S. Zhang, *Sep. Purif. Technol.* **2024**, *331*, 125704.
[15] W. Zhang, P. Jiang, Y. Wang, J. Zhang, Y. Gao, P. Zhang, *RSC Adv.* **2014**, *4*, 51544.
[16] a) L. Zhang, L. Wang, N. Wang, H. Guo, W.-H. Zhang, X. Li, S. Ji, Q.-F. An, *J. Membr. Sci.* **2020**, *598*, 117652; b) H. Jiang, Y. Chen, S. Song, Z. Guo, Z. Zhang, C. Zheng, G. He, H. Wang, H. Wu, T. Huang, Y. Ren, X. Liu, J. Zhang, Y. Yin, Z. Jiang, M. D. Guiver, *Chem. Eng. J.* **2022**, *439*, 135657.
[17] X. Q. Ran, H. L. Qian, X. P. Yan, *Anal. Chem.* **2022**, *94*, 8533.
[18] a) Y.-C. Liu, L.-H. Yeh, M.-J Zheng, K. C.-W. Wu, *Sci. Adv.* **2021**, *7*, eabe9924; b) X. Yu, C. Li, J. Chang, Y. Wang, W. Xia, J. Suo, X. Guan, V. Valtchev, Y. Yan, S. Qiu, Q. Fang, *Angew. Chem., Int. Ed.* **2022**, *61*, 202200820; c) L. Zhai, Y. Yao, B. Ma, M. M. Hasan, Y. Han, L. Mi, Y. Nagao, Z. Li, *Macromol. Rapid Commun.* **2022**, *43*, e2100590.
[19] C. Yuan, X. Wu, R. Gao, X. Han, Y. Liu, Y. Long, Y. Cui, *J. Am. Chem. Soc.* **2019**, *141*, 20187.
[20] X. Sun, M. Di, J. Liu, L. Gao, X. Yan, G. He, *Small* **2023**, *19*, 2303757.
[21] S. Zhang, J. Zhou, H. Li, *Angew. Chem., Int. Ed.* **2022**, *61*, 202204012.
[22] Y. Huang, H. Zeng, L. Xie, R. Gao, S. Zhou, Q. Liang, X. Zhang, K. Liang, L. Jiang, B. Kong, *J. Am. Chem. Soc.* **2022**, *144*, 13794.
[23] a) K. Dey, M. Pal, K. C. Rout, H. S. Kunjattu, A. Das, R. Mukherjee, U. K. Kharul, R. Banerjee, *J. Am. Chem. Soc.* **2017**, *139*, 13083; b) S.-L. Zhang, B.-B. Li, A.-Q. Liu, L.-X. Xie, Z.-F. Li, G. Li, *Coord. Chem. Rev.* **2024**, *507*, 215748.
[24] C.-Y. Zheng, H.-L. Qian, C. Yang, X.-Q. Ran, X.-P. Yan, *ACS Sens.* **2023**, *8*, 4747.
[25] X. Zhang, M. Lin, Y. Dai, F. Xia, *Anal. Chem.* **2023**, *95*, 10465.
[26] a) J. C. Wang, X. Kan, J. Y. Shang, H. Qiao, Y. B. Dong, *J. Am. Chem. Soc.* **2020**, *142*, 16915; b) B. Hou, S. Yang, K. Yang, X. Han, X. Tang, Y. Liu, J. Jiang, Y. Cui, *Angew. Chem., Int. Ed.* **2021**, *60*, 6086; c) X. Kang,

E. R. Stephens, B. M. Spector-Watts, Z. Li, Y. Liu, L. Liu, Y. Cui, *Chem. Sci.* **2022**, *13*, 9811.
[27] Y. Yan, X. Li, G. Chen, K. Zhang, X. Tang, S. Zhang, S. Zheng, J. Fan, W. Zhang, S. Cai, *Chin. Chem. Lett.* **2021**, *32*, 107.
[28] X. Han, J. Zhang, J. Huang, X. Wu, D. Yuan, Y. Liu, Y. Cui, *Nat. Commun.* **2018**, *9*, 1294.
[29] a) Y. Li, Q. Wu, X. Guo, M. Zhang, B. Chen, G. Wei, X. Li, X. Li, S. Li, L. Ma, *Nat. Commun.* **2020**, *11*, 599; b) M. C. Daugherty, E. Vitaku, R. L. Li, A. M. Evans, A. D. Chavez, W. R. Dichtel, *Chem. Commun.* **2019**, *55*, 2680.
[30] M. Y. Wu, R. J. Mo, X. L. Ding, L. Q. Huang, Z. Q. Li, X. H. Xia, *Small* **2023**, *19*, e2301460.
[31] X. Q. Ran, H. L. Qian, X. P. Yan, *Anal. Chem.* **2021**, *93*, 14287.
[32] L. Cao, X. Liu, D. B. Shinde, C. Chen, I. C. Chen, Z. Li, Z. Zhou, Z. Yang, Y. Han, Z. Lai, *Angew. Chem., Int. Ed.* **2022**, *61*, 202113141.
[33] J. Liu, G. Han, D. Zhao, K. Lu, J. Gao, T. Chung, *Sci. Adv.* **2020**, *6*, eabb1110.
[34] a) S. Wang, Y. Chen, Z. Gao, M. Xiong, Z. Zhong, L. Ye, *J. Pharm. Biomed. Anal.* **2007**, *44*, 1095; b) T. Wen, M. Sang, M. Wang, L. Han, Z. Gong, X. Tang, X. Long, H. Xiong, H. Peng, *Sens. Actuators, B* **2021**, *328*, 129048; c) J. Völkle, K. Kumpf, A. Feldner, P. Lieberzeit, P. Fruhmann, *Sens. Actuators, B* **2022**, *356*, 131293; d) T. Wen, Q. Nie, L. Han, Z. Gong, D. Li, Q. Ma, Z. Wang, W. He, L. Wen, H. Peng, *Food Chem.* **2022**, *387*, 132905.